

Article

Polysynthetic Twinning of Diopsides in the Niewang and Tatliksu Nephrite Deposits, Xinjiang, China

Huan Liang ¹, Guanghai Shi ^{1,*}, Ye Yuan ¹, Chuqi Cao ^{1,2}, Xiang Sun ¹ and Xiaohui Zhang ³

¹ State Key Laboratory of Geological Processes and Mineral Resources, China University of Geosciences, Beijing 100083, China

² Institute of Geology, Chinese Academy of Geological Sciences, Beijing 100037, China

³ Beijing Institute of Economics and Management, Beijing 100018, China

* Correspondence: shigh@cugb.edu.cn; Tel.: +86-010-8232-1836

Abstract: Diopside, an important component of the crustal and upper mantle, plays an important role in the formation of nephrite. Polysynthetic twinning in natural diopside, especially from skarns, has rarely been systematically researched. Here, the polysynthetic twinning of natural diopside was investigated in two skarn-type nephrite deposits (Niewang and Tatliksu) in Qiemo, Xinjiang, China. Petrographic observations revealed periodic alternations of dark–light lamellae under cross-polarized light and parallel striations under plane-polarized light, whereas backscattered electron images indicated high homogeneity, which suggested a type of mechanical polysynthetic twinning. According to the optical indicatrix, twins were predominantly oriented as a (100)[100] system. Raman spectra and chemical data show that pyroxenes in nephrite are close to the Di end-member with 0.90–1.04 a.p.f.u. Mg and 0.98–1.05 a.p.f.u. Ca. Both diopside and tremolite from Tatliksu contain slightly higher Fe than those from Niewang. Given the seismic origin of mechanical clinopyroxenes twins, twins of studied diopsides are likely to be attributed to Paleozoic–Mesozoic paleoearthquakes in the Altyn Mountain. A shear stress ≥ 140 MPa and a differential stress greater than 280 MPa are suggested as conditions linked to generation of the twinning of diopsides in the nephrite deposits. The replacement of diopside by tremolite along its twin planes highlights the potential gemological implications, as such replacement by tremolite probably facilitated the formation of dense, fine fibre textures in the nephrites.

Keywords: mechanical polysynthetic twin; diopside; tremolite; skarn; Altyn Mountain; seismic shear deformation



Citation: Liang, H.; Shi, G.; Yuan, Y.; Cao, C.; Sun, X.; Zhang, X. Polysynthetic Twinning of Diopsides in the Niewang and Tatliksu Nephrite Deposits, Xinjiang, China. *Minerals* **2022**, *12*, 1575. <https://doi.org/10.3390/min12121575>

Academic Editor: Luca Bindi

Received: 2 October 2022

Accepted: 5 December 2022

Published: 8 December 2022

Publisher's Note: MDPI stays neutral with regard to jurisdictional claims in published maps and institutional affiliations.



Copyright: © 2022 by the authors. Licensee MDPI, Basel, Switzerland. This article is an open access article distributed under the terms and conditions of the Creative Commons Attribution (CC BY) license (<https://creativecommons.org/licenses/by/4.0/>).

1. Introduction

Diopside, a variety of clinopyroxene, is widely distributed in different kinds of rocks. It is an important component of the crustal and upper mantle, of ultrabasic and basic composition, and of hydrothermal and magmatic origin. It is also a characteristic product of the thermal metamorphism of a silicious carbonate protolith, as it commonly coexists with garnet, vesuvianite, wollastonite, amphibole, and calcite in skarns [1]. Nephrites in the Kunlun–Altyn Mountain are reported to be skarn-related [2–5]. Despite its frequent replacement by tremolite, diopside is commonly found throughout most domains of nephrite deposits, and thus, it is assigned an important role in the formation of nephrite [2–6].

Polysynthetic twinning is multiple single crystals that are parallel with each other along composition planes. The alternating crystals have the same crystallographic orientation. It is a widespread deformation mechanism in minerals with low symmetry, including carbonate minerals, plagioclase and clinopyroxene [7–9]. There is a high energy associated with octahedral skew reversals in diopside, where the M2 site is occupied by larger cations such as Ca²⁺ [10]. Therefore, such mechanical twinning of diopside is theoretically favorable; however, it is infrequently reported in nature [11–15].

Several cases of diopside deformation twinning have been reported as a result of shock loading in meteorites [16] or as the product of experiments conducted under high pressures [9,17–19]. Only a few studies on the polysynthetic twinning in terrestrial clinopyroxene are available [20–22], and the crystals researched in existing studies are much closer to the hedenbergite end-member than to diopside. Even though diopside is common in the nephrite deposits, its twinning has not been frequently observed; only two exceptions were mentioned by Gil et al. [23] and Cooper [6]. In this study, the polysynthetic twinning of diopside in skarn-type nephrite deposits in Qiemo, Xinjiang, China is examined.

2. Geological Setting

Diopsides exhibiting polysynthetic twinning were found in two nephrite deposits in Qiemo County, China (Niewang at N38°00.224', E87°18.226' and Tatliksu at N37°52.537', E86°25.061'; Figure 1).

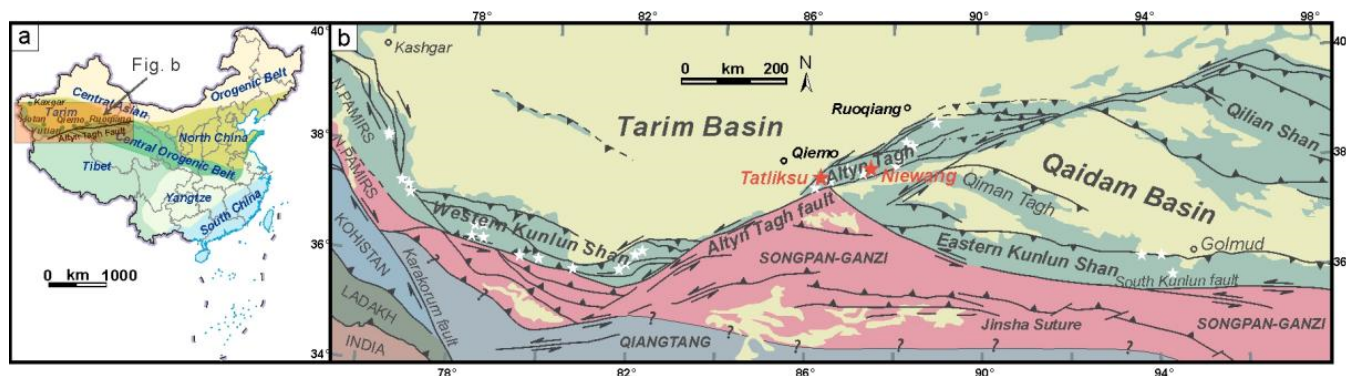


Figure 1. (a) Distribution of major tectonic units in China, modified after the outline map of China [censor code of GS(2019)1651] from the Ministry of Natural Resources of China; (b) Schematic geological map of the northern Tibetan Plateau and the distribution of primary nephrite deposits in Altyn Tagh, Western Kunlun and Eastern Kunlun (stars in white and red). The Niewang and Tatliksu nephrite deposits (stars in red) located in Altyn Tagh and near the Altyn Tagh Fault (ATF), modified after [3,24,25].

Geologically, the two deposits are located in the Altyn Mountain. They belong to the South Altyn Tagh subduction–collision complex, which lies between the Tarim and Qaidam basins and marks the northern margin of the Qinghai–Tibet Plateau (Figure 1).

Chronologically, the strata in the Altyn complex comprises the Archean Milan Group, the Palaeoproterozoic Altyn Group and the Mesoproterozoic Taxidaban Group [25]. It consists predominantly of crystalline schist, migmatitic gneiss, dolomitic marble and other metasedimentary rocks, which unconformably contact with the overlying Cambrian layered siltstones. Magmatic activities were frequent during the Hercynian Period [26,27], and granite, diorite, tonalite, and moyite occurred predominantly. The most significant tectonic deformation today is the Altyn Tagh Fault (ATF), which is a NEE-striking left-lateral strike-slip fault [28,29]. The ATF separates West Kunlun and East Kunlun, as well as Altyn Tagh and the Qaidam Basin, and it significantly affects nephrite mineralization and distribution [2–5,29,30]. Secondary faults have provided channels for hydrothermal activities and closely constrained the formation of nephrite deposits.

The Niewang deposit is mainly associated with the strata of the Altyn Group, which are dominated by migmatitic gneiss intercalated with dolomite marble. The strata exhibit a NE strike and dip angles of 80°–85°; they are 300–500 m long and 2–10 m wide [29]. Normal faults distributed in the contact zone between migmatitic gneiss and dolomitic marble are closely related to mineralization (Figure 2b). The Tatliksu deposit contains 14 ore bodies. The white-gray to gray nephrite bodies almost vertically appear along the contact zone of dolomitic marbles and monzogranites, which are 5–20 m long and only tens of cm thick

(Figure 2a). Their shapes—which were restricted by the outline of dolomite marbles—are irregular massive, veined, lentoid and layered.

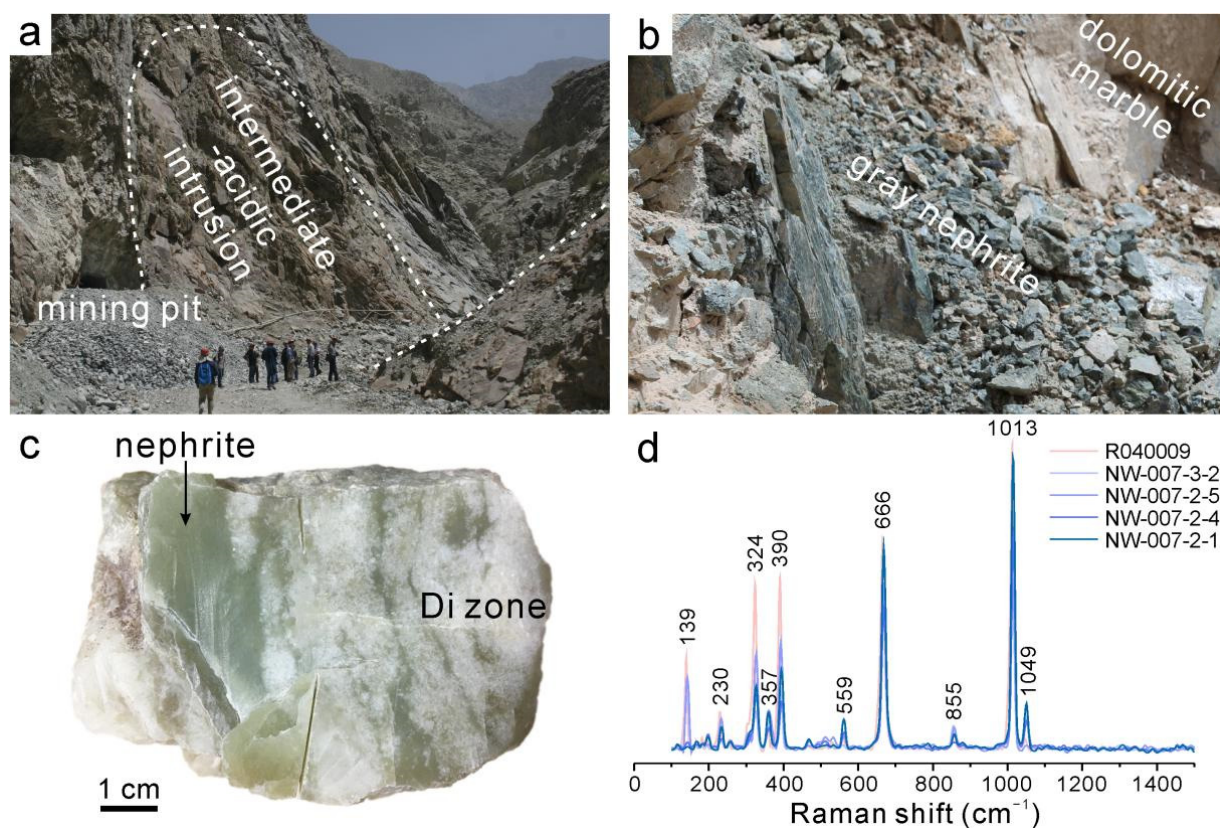


Figure 2. (a) Photograph of intermediate-acidic intrusions near a nephrite orebody at the Tatliksu nephrite deposit; (b) Photograph of an outcrop showing gray nephrite in contact with dolomitic marble at the Niewang deposit, view of picture is about 3 m in length; (c) Photograph of nephrite with massive and veined colorless-white diopside crystals in a sample QMNW-007 from Niewang; (d) Raman spectra of reference diopside R040009 and the diopsides in the sample QMNW-007 in (c).

Caledonian granodiorites occur frequently in these two deposits. The dolomitic marble is strongly altered at the contact zone and fractures. The mineral assemblage zones are characterized as: calcite-bearing dolomitic marble → nephrite → epidote-altered diopsidite → slightly epidote-altered granodiorite and syenite, similar to those of the Saidikulam deposit [5]. However, due to the sedimentary cover, the zoning in the studied area is not as distinctive as that in the Saidikulam deposit.

3. Methods

Conventional gemological tests, micro-observations and Raman spectroscopy measurements were performed at the Experimental Teaching Center of Gemology, China University of Geosciences, Beijing (CUGB). The presence or absence of twinning was investigated using polished thin sections under an Olympus BX51 polarizing microscope. Regarding the Raman spectra, a Horiba HR-Evolution Laser Raman micro-spectrometer was utilized. It was operated using a laser with a wavelength (λ) of 532 nm as the excitation source, and samples were scanned from 100 to 4000 cm^{-1} . Before measurement, monocrystalline silicon with a Raman shift at 520.7 cm^{-1} was used for calibration [31]. The laser scanned for 10 s, which cumulated 5 times at a spot of approximately 1 μm with an entrance slit of 100 μm .

Chemical compositions and backscattered electron (BSE) images were obtained using an electron probe microanalyzer (EPMA-1720, Shimadzu Corporation, Kyoto, Japan) in the Laboratory Center at CUGB. The beam current, accelerating voltage, count time and

beam size at which the instrument was operated were 10 nA, 15 kV, 10 s and 5 μm , respectively. The atomic number Z X-ray absorption and the X-ray fluorescence effect (ZAF) program were used for correction. The standards that were used for calibration included the following: olivine for Mg, diopside for Si and Ca, chromite for Fe and Cr, albite for Na and Al, K-sanidine for K, rutile for Ti, rhodonite for Mn and pentlandite for Ni.

4. Results

4.1. Gemological Properties

Among a certain type of smooth nephrite stone, there is occasionally a white stone-like (drier luster) appearance in one or more domains. The jade dealers refer to such a domain as “Jiang (疆)”. In this study, “Jiang” means to be composed of coarse-grained diopsides, as opposed to the fine-grained greasy domains of nephrite. These diopside crystals are granular when viewed with the naked eye, and they stack together in the form of a line or mass in and/or very close to white-gray nephrite (Figure 2c).

4.2. Raman Spectra

Diopside in the samples we studied exhibited Raman shifts at approximately 139, 230, 324, 357, 390, 559, 666, 1013 and 1049 cm^{-1} , which are values consistent with the standard diopside (RRUFFID = R040009, Figure 2d). Most of the peaks are ascribed to $[\text{Si}_2\text{O}_6]^{4-}$, with the 1013 cm^{-1} peak attributed to the symmetric stretching vibration of Si–O. The peaks at 666 cm^{-1} are linked to the symmetric bending vibration of Si–O–Si, whereas the asymmetric bending vibrations of Si–O–Si are associated with the peaks at 390 and 324 cm^{-1} . The weak peaks at 559, 230 and 357 cm^{-1} are coupled bands of the M–O stretching vibration and the Si–O–Si bending vibration.

4.3. Petrography

In the studied deposits, diopsides occur in the nephrite and contact zones. Nephrite consists of cryptocrystalline tremolite and minor relicts of diopside, prehnite and granular apatite. The contact zone comprises granular diopside and titanite, aggregates of epidote, and tremolite. Tremolites in the contact zone mainly exhibit two types of microfabrics: coarse-foliated (0.1–3.0 mm) and fine-fibrous. Some tremolite fibers adjacent to twinned diopside were curved. Aggregated epidotes display an emerald-green to lemon-yellow abnormal interference color (Figure 3e) and inhomogeneous brightness in the BSE images.

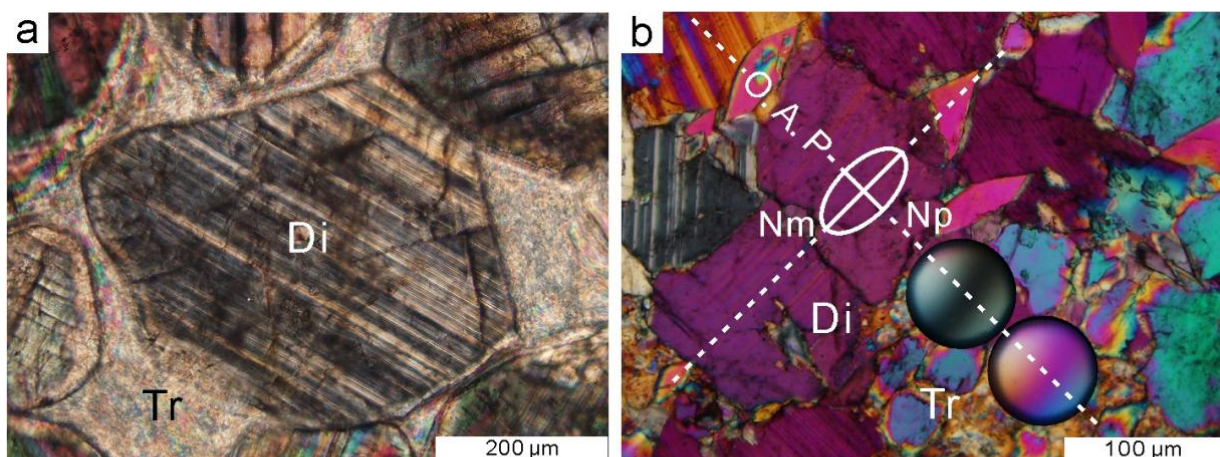


Figure 3. Cont.

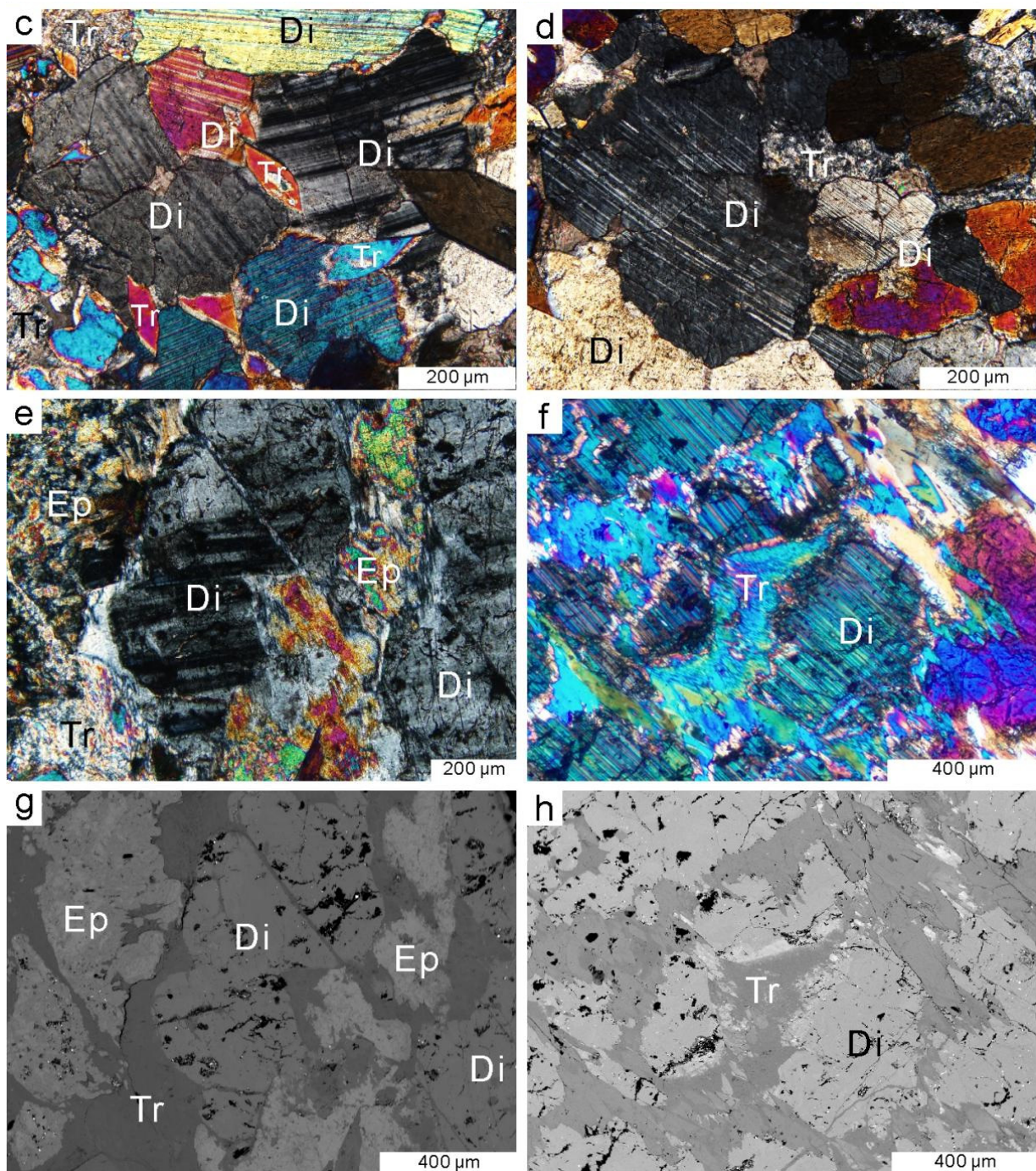


Figure 3. Micropetrography photos (a–f) and BSE images (g,h): (a) Twinned diopsides very close to nephrite from the sample in Figure 2c; (b) Optical indicatrix determination involving the insertion of a gypsum plate, the twinning planes are parallel to the Nm optical axis; (c–f) Twinned diopsides in the contact zone from Tatliksu exhibit alternations of bright and dark bands. Some twin lamellae and nearby tremolite fibers are curved; (g,h) the same domain in (e) and (f), respectively. Each individual diopside twin displays identical brightness in BSE images, showing no obvious chemical change. Di—diopside; Ep—epidote; Tr—tremolite; Ng, Nm and Np—optical axis, $Ng > Nm > Np$; O.A.P—optical axial plane.

Twinned diopside crystals are found in the epidote-altered diopsidite zone and occur as fine strips or small blocks in nephrites. Their grains vary in size from 0.2 to 2.0 mm and range from colorless to light-brown with slightly round boundaries. Some diopsides

(ca. 20%) display alternating bright and dark bands under cross-polarized light and corresponding parallel striations under plane-polarized light (Figure 3). These striations are straight and consecutive in the direction of elongation. In the BSE images, they show the same brightness (Figure 3e–h), excluding even a slight chemical change. Individual odd or even lamellae show alternating extinctions, and adjacent lamellae show extinctions at intervals of approximately 30–60°. The simultaneous extinctions of interphase lamellae indicate an identical crystallographic orientation. These observations allow for the suggestion of polysynthetic twinning. These thin twin lamellae are commonly <50 µm in width. Some twin lamellae and nearby tremolite fibers were found to be curved, implying stress after the formation of diopside twins.

Square or octagonal basal sections revealed a group of microcracks that are nearly perpendicular, corresponding to the {110} cleavage of diopside (87°, Figure 3a). These cracks stretch for 200–400 µm and are approximately 100–200 µm apart. In addition, many samples exhibited microcracks perpendicular to the extension direction. In most cases, twin striations and cleavages/cracks were found to display oblique crossings.

4.4. Mineral Chemistry

Pyroxenes in the nephrite deposits contain 0.90–1.04 a.p.f.u. Mg and 0.98–1.05 a.p.f.u. Ca, indicating a composition close to the diopside end-member (Table 1 and Figure 4a) [32]. The contents of (Fe²⁺ + Fe³⁺) show minor variation, with a maximum of 0.21 a.p.f.u. (up to 21 mol.% hedenbergite end-member). Diopsides from the Tatliksu deposit (0.067–0.207 a.p.f.u.) yield higher concentrations of Fe ions compared to those from Niewang (up to 0.008 a.p.f.u.). They differ from those reported twinned diopsides from other types of rocks [20].

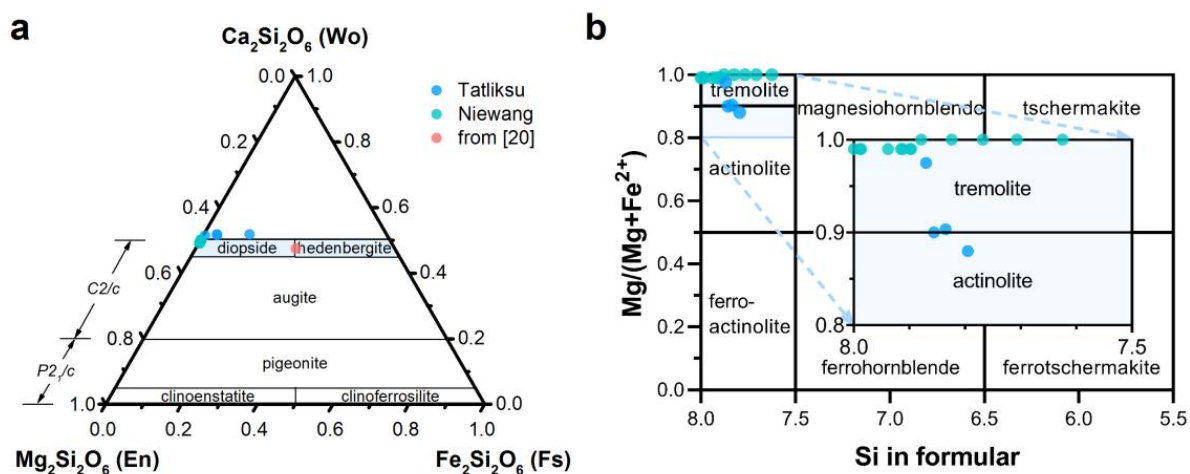


Figure 4. (a) Plot of the Ca-Mg-Fe composition of clinopyroxenes with polysynthetic twinning based on Wo-En-Fs (mol.) ternary classification [32]; (b) Classification diagram of surrounding amphiboles, after Leake et al. [33] and Hawthorne et al. [34].

Based on the classification scheme of the amphibole supergroup [33,34], most amphiboles in this study are tremolites (see Table 2 and Figure 4b). Tremolites from Niewang yield Mg contents of 4.84–5.31 a.p.f.u. and Mg[#] [Mg/(Mg + Fe²⁺)] of 0.99–1.00, whereas amphiboles from Tatliksu contain less Mg (4.15–4.75 a.p.f.u.) and Mg[#] (0.88–0.95), partially belonging to actinolite. This is similar to the feature of Mg vs. Fe in the diopsides from the two deposits.

Table 1. Chemical compositions of diopside from the studied nephrite deposits (wt.%) *.

Deposit; Rock Type	Niewang (Close to Nephrite)						Tatliksu (Ep-Di Zone)			
	Sample		007-2		007-3		1		5-9	
No.	1-2	4-1	5	8	5-1	4-1-1	2-4	1-4	1-3	1-2
SiO ₂	55.844	55.111	54.942	54.557	54.295	55.302	54.111	53.820	52.491	52.310
TiO ₂	b.d.l.	0.045	0.027	0.032	0.101	0.012	0.077	b.d.l.	b.d.l.	b.d.l.
Al ₂ O ₃	0.052	0.112	0.115	0.364	0.095	0.087	0.120	0.188	0.362	0.121
Cr ₂ O ₃	0.026	b.d.l.	b.d.l.	0.027	b.d.l.	b.d.l.	0.045	n.a.	n.a.	n.a.
FeO	0.020	0.083	0.118	0.203	0.083	b.d.l.	0.177	2.280	2.170	6.527
MnO	0.055	0.029	b.d.l.	0.049	b.d.l.	0.002	0.092	0.129	0.118	1.146
NiO	b.d.l.	0.018	b.d.l.	0.010	0.061	0.059	0.038	b.d.l.	b.d.l.	b.d.l.
MgO	18.430	18.613	18.940	18.844	19.401	18.100	18.651	16.458	16.305	12.798
CaO	25.724	25.314	26.499	25.861	26.142	25.373	25.877	26.404	26.307	25.576
Na ₂ O	0.030	0.015	0.029	0.075	0.048	0.018	0.044	0.095	0.124	0.133
K ₂ O	b.d.l.	0.016	b.d.l.	0.010	0.004	0.004	0.010	b.d.l.	0.004	b.d.l.
Total	100.181	99.356	100.67	100.032	100.23	98.957	99.242	99.374	97.881	98.611
Si	2.01	2.00	1.96	1.96	1.95	2.02	1.96	1.97	1.95	1.98
AlIV	0.00	0.00	0.00	0.02	0.00	0.00	0.01	0.01	0.02	0.01
Fe ³⁺	0.00	0.00	0.00	0.01	0.00	0.00	0.01	0.02	0.03	0.00
Sum T	2.01	2.00	1.97	1.99	1.95	2.02	1.98	2.00	2.00	1.99
Fe ³⁺	0.00	0.00	0.00	0.00	0.00	0.00	0.00	0.03	0.04	0.04
Fe ²⁺	0.00	0.00	0.00	0.00	0.00	0.00	0.00	0.02	0.00	0.16
Mn	0.00	0.00	0.00	0.00	0.00	0.00	0.00	0.00	0.00	0.04
Mg	0.99	0.99	1.00	1.00	1.00	0.98	1.00	0.90	0.90	0.72
Sum M1	0.99	0.99	1.00	1.00	1.00	0.98	1.00	0.95	0.94	0.96
Mg	0.00	0.01	0.01	0.01	0.04	0.00	0.01	0.00	0.00	0.00
Ca	0.99	0.98	1.02	1.00	1.00	0.99	1.01	1.04	1.05	1.04
Na	0.00	0.00	0.00	0.01	0.00	0.00	0.00	0.01	0.01	0.01
Sum M2	0.99	1.00	1.03	1.01	1.05	0.99	1.02	1.04	1.06	1.05
Di	1.00	1.00	1.00	0.99	1.00	1.00	0.99	0.93	0.93	0.79
Hed	0.00	0.00	0.00	0.01	0.00	0.00	0.01	0.07	0.07	0.21

* The pyroxene formulae were calculated on the basis of 4 cations and 6 oxygens; Fe³⁺ and Fe²⁺ were estimated by charge balance; b.d.l.—below detection limit, n.a.—not analyzed.

Table 2. Chemical compositions of tremolite-actinolite from the studied nephrite deposits (wt.%) *.

Deposit and Rock Type	Niewang (Nephrite)			Tatliksu (Ep-Di Zone)			
	Sample and No.	7-2-2	7-2-4-3	7-3-5	1-1-2	1-3-2	1-1-3
SiO ₂		56.792	58.090	57.439	54.851	55.098	54.771
TiO ₂		0.067	0.027	0.002	0.157	b.d.l.	0.078
Al ₂ O ₃		1.499	1.156	1.204	1.009	1.628	2.563
Cr ₂ O ₃		0.084	b.d.l.	b.d.l.	n.a.	n.a.	n.a.
Fe ₂ O ₃		0.672	0.302	0.435	0.483	0.140	0.000
FeO		0.606	0.555	0.392	4.471	4.040	4.848
MnO		0.081	0.080	0.067	0.140	0.140	0.098
NiO		0.001	0.108	0.017	b.d.l.	0.016	0.014
MgO		24.673	24.239	24.904	20.400	20.569	19.555
CaO		13.282	12.297	13.309	13.721	13.627	13.526
Na ₂ O		0.229	0.119	0.175	0.110	0.204	0.322
K ₂ O		0.261	0.367	0.143	0.055	0.089	0.150
Total		98.247	97.340	98.087	95.397	95.551	95.925

Table 2. Cont.

Deposit and Rock Type	Niewang (Nephrite)			Tatliksu (Ep-Di Zone)			
	Sample and No.	7-2-2	7-2-4-3	7-3-5	1-1-2	1-3-2	1-1-3
Si		7.71	7.91	7.77	7.86	7.84	7.80
Al ^{IV}		0.24	0.09	0.19	0.14	0.16	0.20
Ti		0.01	0.00	0.00	0.00	0.00	0.00
Fe ³⁺		0.04	0.00	0.04	0.00	0.00	0.00
Sum T		8.00	8.00	8.00	8.00	8.00	8.00
Al ^{VI}		0.00	0.10	0.00	0.03	0.11	0.23
Cr		0.01	0.00	0.00	0.00	0.00	0.00
Ti		0.00	0.00	0.00	0.02	0.00	0.01
Fe ³⁺		0.03	0.03	0.00	0.05	0.02	0.00
Mg		4.91	4.86	4.96	4.36	4.36	4.15
Fe ²⁺		0.00	0.00	0.00	0.47	0.48	0.58
Mn		0.01	0.01	0.00	0.02	0.02	0.01
Ca		0.00	0.00	0.00	0.04	0.01	0.02
Sum C		5.00	5.00	5.00	5.00	5.00	5.00
Mg		0.09	0.06	0.06	0.00	0.00	0.00
Ni		0.00	0.01	0.00	0.00	0.00	0.00
Fe ²⁺		0.00	0.03	0.00	0.00	0.00	0.00
Mn		0.00	0.00	0.01	0.00	0.00	0.00
Ca		1.91	1.80	1.93	2.00	2.00	2.00
Na		0.00	0.03	0.00	0.00	0.00	0.00
Sum B		2.00	1.93	2.00	2.00	2.00	2.00
Ca		0.02	0.00	0.00	0.02	0.03	0.01
Na		0.03	0.00	0.05	0.03	0.06	0.09
K		0.05	0.06	0.03	0.01	0.02	0.03
Sum A		0.10	0.06	0.08	0.06	0.11	0.13
Mg/(Mg + Fe ²⁺)		1.00	0.99	1.00	0.90	0.90	0.88
Mineral		Tr	Tr	Tr	Tr	Tr	Act

* Amphibole formulae were calculated using the software MINPET 2.0 on the basis of 23 oxygen atoms and 13 small cations (excluding Ca, Na and K). The Fe₂O₃ contents and total contents were recalculated based on the results for Fe³⁺. B.d.l.—below detection limit; n.a.—not analyzed.

5. Discussion

5.1. Determination of the Twinning Law

Parallel lamellae could also be observed in some pyroxenes, and this is attributable to exsolution [35]. However, this explanation can be easily excluded from polysynthetic twinning because of the following distinguishing characteristics: 1. Lamellae that are linked to exsolution are commonly parallel to the host crystal, which displays a parallel extinction, while the extinction relative to twinning planes is oblique. 2. Exsolution lamellae usually terminate at a short distance from the boundary of the host crystal and are frequently curved at their termination, while twinning planes extend across the entire grain. 3. Exsolved lamellae show varying chemical compositions, and thus, the corresponding BSE images are inhomogeneous. Therefore, the observed patterns of the diopsides in the studied nephrite deposits are considered to be polysynthetic twinning. Owing to other frequent brittle-ductile deformations of diopside and some adjacent tremolite fibers (curved, Figure 3), this polysynthetic twinning is more likely to be a mechanical one.

Raleigh and Talbot [11] and Kirby and Christie [18] determined the twin glide elements for two mechanical twins of diopside to be (100)[001] and (001)[100] based on the transmission electron microscopy observations. Subsequently, several laboratory deformation experiments confirmed the (100)[001] glide system was preferentially activated in clinopyroxenes [8,9,19,36,37], while (001)[100] twins originated from growth instead of shock deformation [16].

In this study, the twinning law was determined by an optical indicatrix using a condenser, Bertrand lens and a gypsum plate (Figure 3b). Based on the interference pattern

under the condenser and Bertrand lens, the optical axial plane (O.A.P) was identified. Then, as the normal direction of the O.A.P, the Nm optical direction could also be determined. After the insertion of a gypsum plate, the interference color for areas at the protruding direction of the black arc changed from I-gray to II-blue, implying a radius with the same name as the inserted plate (Np). Further, it was deduced that the composition planes of twins were nearly perpendicular to the Np and parallel to the Nm. It is known that the Nm optical axis of diopside coincides with the crystallographic b-axis, and the Np is near the a-axis with an angle of 22°–32°. Therefore, the main law for the polysynthetic twinning of diopside in the nephrite deposit can be inferred as (100)[001]. This conclusion is in agreement with the findings from [8,9,19,36,37].

5.2. Estimation of P-T Conditions

Experimental studies on the deformation of single clinopyroxenes (diopside; hedenbergite [19,36,38–40]; spodumene [41]) and polycrystalline aggregates (eclogites [14,42]; clinopyroxenites [43]; and jadeitites [8,9]) indicated a low–moderate temperature, a moderate-high stress, and/or a very high strain rate associated with the major deformation process for clinopyroxene twinning. As the required stress was confirmed to be almost insensitive to the temperature, strain rate and water content [19,36,44], twinned diopsides can be used as a geobarometer to estimate the magnitude of the shear stress experienced by host rocks.

Kollé and Blacic [19] indicated a homogeneous stress field and an average critical resolved shear stress (CRSS, σ_{res}) for the (100)[001] mechanical twinning of chrome diopside and hedenbergite of 100 ± 30 and 140 ± 10 MPa, respectively. These values were comparable to those for jadeite (150 ± 5 MPa) [9]. Among these, the low values and wide scatter in the data for chrome diopside are attributable to numerous inclusions and (001) growth twins. Thus, a CRSS in the range of 140–150 MPa is considered a more reasonable twinning stress for clinopyroxenes. Then, a minimum differential stress (σ_1 - σ_3) of 280 MPa can be calculated based on the following equation [9]:

$$\sigma_{res} = (\sigma_1 - \sigma_3) (\cos\gamma \cdot \cos\theta) \iff (\sigma_1 - \sigma_3) = \sigma_{res} / (\cos\gamma \cdot \cos\theta) \quad (1)$$

where γ is the angle between the inferred σ_1' direction and the normal to the (100) plane, and θ is the angle between σ_1' and [001]. Additionally, experiments on the twinning of clinopyroxenes have even attained differential stresses greater than 0.5 GPa (possibly even up to 1 GPa) [8,19]. Therefore, these diopside twins in nephrites recorded a peak stress of at least 0.28 GPa—even up to 1 GPa—after the formation of diopside, a value which is considerably higher than the pressure related to the formation of nephrite (100–200 MPa [45]).

5.3. Genesis of Mechanical Twinning of the Diopside

In contrast to calcites and feldspars, mechanical twinning is rare in pyroxenes. Analyses of the crystal structures suggested that the formation of twins of diopside along (100) involved a partial dislocation of the Burgers vector $c/2$ in the (100) octahedral layers, which resulted from a quasi-instantaneous deviatoric stress on (100) planes in the [001] direction [17]. In general, these are considered signatures of strong shock events, such as shocks from meteorites [19,38,46–48] and shocks generated in the laboratory statically [17,18] or tectonically [36,38]. In terrestrial clinopyroxenes, such shocks were found to be rare, unless there was a quasi-instantaneous loading that was attributable to the stress redistribution during a major seismic event [8,9,11,49,50].

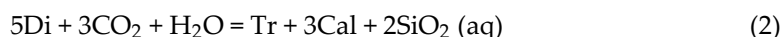
The ATF is one of the few great active strike-slip faults worldwide. It is also one of the major seismically active belts in China and is regarded as a natural laboratory for earthquake behavior research [51]. Multiple complex geological evolution processes, such as oceanic crust subduction, exhumation and collision orogeny during the convergence of the Tarim Block and the Proto-Tethys Tectonic System in the Early Paleozoic, triggered a series of intense tectonic deformations [24–29,51–54]. In this region, quite a few paleoearthquakes ranging in occurrence from the Paleozoic to Mesozoic period have been recorded and re-

ported on, e.g., [51,54,55]. The distribution of nephrite deposits in the Kunlun and Altyn Mountains is closely related to the strike-slip fault and shear zone, where the earthquake epicenters are concentrated.

Based on above proofs, the polysynthetic twinning of diopsides in nephrites can be attributed to paleoearthquakes.

5.4. The Influence of Twinned Diopsides on Nephrite Formation

As an important mineral in almost every nephrite deposit, diopside was found to be commonly replaced by tremolite via the following retrograde reaction [56]:



This reaction usually happened along the cleavages, cracks and crystal boundaries of diopside. The polysynthetic twinning of diopside did not generate fractures. However, spaces in the twinning planes between adjacent twinned lamellae also facilitated the replacement of diopside by tremolite. As shown in Figure 3, some tremolite fibers obviously developed parallel to twin striations. This implies that the polysynthetic twinning of diopside can accelerate the replacement of diopside by tremolite and promote a thorough reaction when undergoing the process outlined in Equation (2) above.

6. Conclusions

Diopsides with polysynthetic twinning of the (100), [100] law were found in the nephrite deposits from Qiemo, China. They were close to the Di end-member. The formation of these diopside twins required an average critical resolved shear stress of 140 MPa and a differential stress of at least 280 MPa, conditions which were likely induced by paleoearthquakes. Petrographic observation revealed the replacement of diopside by tremolite, also through its twin lamellae. Therefore, in the long and multi forming stages of the nephrite deposit, this twinning would have accelerated the thorough replacement of diopside by tremolite, which is of potential gemological significance.

Author Contributions: Conceptualization and methodology, H.L. and G.S.; field investigation, G.S. and Y.Y.; experiment, H.L. and C.C.; data analysis, H.L. and G.S.; writing—original draft preparation, H.L. and G.S.; writing—review and editing, H.L., G.S., X.S. and X.Z.; project administration, G.S.; funding acquisition, G.S. All authors have read and agreed to the published version of the manuscript.

Funding: This research was funded by the National Key R&D Program of China (grant no. 2022YFC-2903302), the Second Tibetan Plateau Scientific Expedition and Research Program (STHP) (grant no. 2019QZKK0802) and the National Science Foundation of China (grant no. 42273044).

Data Availability Statement: Not applicable.

Acknowledgments: We thank Shiqi Wang, Xinling Li, Ming Yu and Kong Gao for their kind support during the field investigation; Qingqing Deng for help with the EPMA analyses; Yu Zhang for help with the Raman analyses; Xiangyu Zhang and Linjing Zhang for help with the selection of laboratories.

Conflicts of Interest: The authors declare no conflict of interest.

References

1. Oyman, T. Geochemistry, mineralogy and genesis of the Ayazmant Fe-Cu skarn deposit in Ayvalik, (Balikesir), Turkey. *Ore Geol. Rev.* **2010**, *37*, 175–201. [[CrossRef](#)]
2. Liu, Y.; Deng, J.; Shi, G.H.; Yui, T.-F.; Zhang, G.B.; Abuduwayiti, M.; Yang, L.Q.; Sun, X. Geochemistry and petrology of nephrite from Alamas, Xinjiang, NW China. *J. Asian Earth Sci.* **2011**, *42*, 440–451. [[CrossRef](#)]
3. Gao, K.; Shi, G.H.; Wang, M.L.; Xie, G.; Wang, J.; Zhang, X.C.; Fang, T.; Lei, W.Y.; Liu, Y. The Tashisayi nephrite deposit from South Altyn Tagh, Xinjiang, northwest China. *Geosci. Front.* **2019**, *10*, 1597–1612. [[CrossRef](#)]
4. Jiang, Y.; Shi, G.; Xu, L.; Li, X. Mineralogy and Geochemistry of Nephrite Jade from Yinggelike Deposit, Altyn Tagh (Xinjiang, NW China). *Minerals* **2020**, *10*, 418. [[CrossRef](#)]

5. Zhang, X.C.; Shi, G.H.; Zhang, X.M.; Gao, K. Formation of the nephrite deposit with five mineral assemblage zones in the Central Western Kunlun Mountains, China. *J. Petrol.* **2022**, *63*, egac117. [[CrossRef](#)]
6. Cooper, A.F. Origin and evolution of nephrites, diopsidites and giant diopside crystals from the contact zones of the Pounamu Ultramafics, Westland, New Zealand. *N. Z. J. Geol. Geophys.* **2022**, 1–14. [[CrossRef](#)]
7. Stark, J.P. Mechanical twinning in crystals. *Phys. Rev. B* **1998**, *38*, 1139–1142. [[CrossRef](#)]
8. Trepmann, C.; Stöckhert, B. Mechanical twinning of jadeite—An indication of synseismic loading beneath the brittle-plastic transition. *Int. J. Earth Sci.* **2001**, *90*, 4–14. [[CrossRef](#)]
9. Orzol, J.; Trepmann, C.; Stöckhert, B.; Shi, G.H. Critical shear stress for mechanical twinning of jadeite—An experimental study. *Tectonophysics* **2003**, *372*, 135–145. [[CrossRef](#)]
10. Smyth, J.R. Experimental study on the polymorphism of enstatite. *Am. Miner.* **1974**, *59*, 345–352.
11. Raleigh, C.; Talbot, J.L. Mechanical twinning in naturally and experimentally deformed diopside. *Am. J. Sci.* **1967**, *265*, 151–165. [[CrossRef](#)]
12. Carter, N.L.; Raleigh, C.B. Principal stress direction from plastic flow in crystals. *Geol. Soc. Am. Bull.* **1969**, *80*, 1231–1264. [[CrossRef](#)]
13. Avé Lallemant, H.G. Experimental deformation of diopside and websterite. *Tectonophysics* **1978**, *48*, 1–27. [[CrossRef](#)]
14. Godard, G.; van Roermond, H. Deformation-induced clinopyroxene fabrics from eclogites. *J. Struct. Geol.* **1995**, *17*, 1425–1443. [[CrossRef](#)]
15. Laurent, P.; Kern, H.; Lacombe, O. Determination of deviatoric stress tensor based on inversion of calcite twin data from experimentally deformed monophase samples: Part ii. Axial and triaxial experiments. *Tectonophysics* **2000**, *327*, 131–148. [[CrossRef](#)]
16. Leroux, H.; Devouard, B.; Cordier, P.; Guyot, F. Pyroxene microstructure in the Northwest Africa 856 martian meteorite. *Meteorit. Planet. Sci.* **2004**, *39*, 711–722. [[CrossRef](#)]
17. Wenk, H.-R. Submicroscopical twinning in lunar and experimentally deformed pyroxenes. *Contrib. Mineral. Petrol.* **1970**, *26*, 315–323. [[CrossRef](#)]
18. Kirby, S.H.; Christie, J.M. Mechanical twinning in diopside $\text{Ca}(\text{Mg,Fe})\text{Si}_2\text{O}_6$: Structural mechanism and associated crystal defects. *Phys. Chem. Miner.* **1977**, *1*, 137–163. [[CrossRef](#)]
19. Kollé, J.J.; Blacic, J.D. Deformation of single-crystal clinopyroxene:1. Mechanical twinning in diopside and hedenbergite. *J. Geophys. Res.* **1982**, *87*, 4019–4034. [[CrossRef](#)]
20. White, A.J.R. Scapolite-Bearing Marbles and Calc-Silicate Rocks from Tungkillo and Milendella, South Australia. *Geol. Mag.* **1959**, *96*, 258–306. [[CrossRef](#)]
21. Tribaudino, M.; Fioretti, A.M.; Martignago, F.; Molin, G. Transmission electron microscope texture and crystal chemistry of coexisting ortho- and clinopyroxene in the Antarctic ureilite Frontier Mountain 90054: Implications for thermal history. *Meteorit. Planet. Sci.* **1997**, *32*, 671–678. [[CrossRef](#)]
22. Zhou, Y.S.; He, C.R. Microstructures and deformation mechanisms of experimentally deformed gabbro. *Earthq. Sci.* **2015**, *28*, 119–127. [[CrossRef](#)]
23. Gil, G.; Barnes, J.D.; Boschi, C.; Gunia, P.; Raczynski, P.; Szakmany, G.; Bendo, Z.; Peterdi, B. Nephrite from Zloty Stok (Sudetes, SW Poland): Petrological, geochemical, and isotopic evidence for a dolomite-related origin. *Can. Mineral.* **2015**, *53*, 533–555. [[CrossRef](#)]
24. Cowgill, E.S.; Yin, A.; Harrison, T.M.S.; Wang, X. Reconstruction of the Altyn Tagh Fault based on U-Pb geochronology: Role of back thrusts, mantle sutures, and heterogeneous crustal strength in forming the Tibetan Plateau. *J. Geophys. Res.-Solid Earth* **2003**, *108*, 2346. [[CrossRef](#)]
25. Zhang, J.X.; Zhang, Z.M.; Xu, Z.Q.; Yang, J.S.; Cui, J.W. Petrology and geochronology of eclogites from the western segment of the Altyn Tagh, northwestern China. *Lithos* **2001**, *56*, 187–206. [[CrossRef](#)]
26. Mao, D.B.; Zhong, C.T.; Niu, G.H.; Zhang, C.S. *A Comprehensive Research Report on Metallogenic Regularity and Prospecting Direction of Altyn Metallogenic Belt in Xinjiang*; Tianjin Geological Survey Center: Tianjin, China, 2003; (In Chinese).
27. Dong, S.L.; Li, Z.; Gao, J.; Zhu, L. Progress of study on Paleozoic tectonic framework and crystalline rock geochronology in Altun- Qilian- Kunlun Orogen. *Geol. Rev.* **2013**, *59*, 731–746, (In Chinese with English Abstract).
28. Wang, C.; Liu, L.; Yang, W.Q.; Zhu, X.H.; Cao, Y.T.; Kang, L.; Chen, S.F.; Li, R.S.; He, S.P. Provenance and ages of the Altyn Complex in Altyn Tagh: Implications for the early Neoproterozoic evolution of northwestern China. *Precambrian Res.* **2013**, *230*, 193–208. [[CrossRef](#)]
29. Wang, S.Q.; Shi, G.H. *Nephrite from Xinjiang, China*; Science Press: Beijing, China, 2022.
30. Liu, Y.; Zhang, R.Q.; Abuduwayiti, M.; Wang, C.; Zhang, S.P.; Shen, C.H.; Zhang, Z.Y.; He, M.Y.; Zhang, Y.; Yang, X.D. SHRIMP U-Pb zircon ages, mineral compositions and geochemistry of placer nephrite in the Yurungkash and Karakash River deposits, West Kunlun, Xinjiang, Northwest China: Implication for a magnesium skarn. *Ore Geol. Rev.* **2016**, *72*, 699–727. [[CrossRef](#)]
31. Shi, G.H.; Zhang, X.C.; Wang, Y.; Li, Q.L.; Wu, F.Y.; He, H.Y. Age determination of oriented rutile inclusions in sapphire and of moonstone from the Mogok metamorphic belt, Myanmar. *Am. Miner.* **2021**, *106*, 1852–1859. [[CrossRef](#)]
32. Morimoto, N.; Fabries, J.; Ferguson, A.K.; Ginzburg, I.V.; Ross, M.; Seifert, F.A.; Zussman, J.; Aoki, K.; Gottardi, G. Nomenclature of pyroxenes. *Am. Miner.* **1988**, *73*, 1123–1133.

33. Leake, B.E.; Woolley, A.R.; Arpes, C.E.S.; Birch, W.D.; Gilbert, M.C.; Grice, J.D.; Hawthorne, F.C.; Kato, A.; Kisch, H.J.; Krivovichev, V.G.; et al. Nomenclature of amphiboles. Report of the Subcommittee on amphiboles of the International Mineralogical Association, Commission on New Minerals and Mineral Names. *Am. Miner.* **1997**, *82*, 1019–1037.
34. Hawthorne, F.C.; Oberti, R.; Harlow, G.E.; Maresch, W.V.; Martin, R.F.; Schumacher, J.C.; Welch, M.D. Nomenclature of the amphibole supergroup. *Am. Miner.* **2012**, *97*, 2031–2048. [[CrossRef](#)]
35. Cameron, M.; Papike, J.J. Structural and chemical variations in pyroxenes. *Am. Miner.* **1981**, *66*, 1–50.
36. Kollé, J.J.; Blacic, J.D. Deformation of single-crystal clinopyroxenes: 2. Dislocation-controlled flow processes in hedenbergite. *J. Geophys. Res.* **1983**, *88*, 2381–2393. [[CrossRef](#)]
37. Leroux, H.; Doukhan, J.C.; Langenhorst, F. Microstructural defects in experimentally shocked diopside: A TEM characterization. *Phys. Chem. Miner.* **1994**, *20*, 521–530. [[CrossRef](#)]
38. Hornemann, U.; Müller, W.F. Shock-induced deformation twins in clinopyroxene. *Neues Jahrb. Mineral. Monatsh.* **1971**, *6*, 247–255.
39. Raterron, P.; Jaoul, O. High-temperature deformation of diopside single crystal. 1. Mechanical data. *J. Geophys. Res.* **1991**, *96*, 14277–14286. [[CrossRef](#)]
40. Ingrin, J.; Doukhan, N.; Doukhan, J.C. Dislocation glide systems in diopside single crystals deformed at 800–900 °C. *Eur. J. Mineral.* **1992**, *4*, 1291–1302. [[CrossRef](#)]
41. Van Duysen, J.C.; Doukhan, N.; Doukhan, J.C. Room temperature microplasticity of alpha-spodumene $\text{LiAlSi}_2\text{O}_6$. *Phys. Chem. Miner.* **1984**, *10*, 125–135. [[CrossRef](#)]
42. Jakubith, M.; Seidel, P. Shock-loading experiments on eclogite. *Geophys. Res. Lett.* **1982**, *9*, 408411. [[CrossRef](#)]
43. Kirby, S.H.; Kronenberg, A.K. Deformation of clinopyroxenite: Evidence for a transition in flow mechanisms and semi-brittle behavior. *J. Geophys. Res.* **1984**, *89*, 3177–3192. [[CrossRef](#)]
44. Tullis, T.E. The use of mechanical twinning in minerals as a measure of shear stress magnitudes. *J. Geophys. Res.* **1980**, *85*, 6263–6268. [[CrossRef](#)]
45. Noh, J.H.; Yu, J.-Y.; Choi, J.B. Genesis of nephrite and associated calc-silicate minerals in Chuncheon area. *J. Geol. Soc. Korea* **1993**, *29*, 199–224. (In Korean)
46. Ashworth, J.R. Deformation mechanisms in mildly shocked chondritic diopside. *Meteoritics* **1980**, *15*, 105–115. [[CrossRef](#)]
47. Müller, W.F. Thermal and deformation history of the Shergotty meteorite deduced from clinopyroxene microstructure. *Geochim. Cosmochim. Acta* **1993**, *57*, 4311–4322. [[CrossRef](#)]
48. Leroux, H.; Jacob, D.; Marinova, M.; Hewins, R.H.; Zanda, B.; Pont, S.; Lorand, J.P.; Humayun, M. Exsolution and shock microstructures of igneous pyroxene clasts in the Northwest Africa 7533 Martian meteorite. *Meteorit. Planet. Sci.* **2016**, *51*, 932–945. [[CrossRef](#)]
49. Skrotzki, W. Defect structure and deformation mechanisms in naturally deformed augite and enstatite. *Tectonophysics* **1994**, *229*, 43–68. [[CrossRef](#)]
50. Shi, G.H.; Wang, X.; Chu, B.B.; Cui, W.Y. Jadeite jade from Myanmar: Its texture and gemmological implications. *J. Gemmol.* **2009**, *31*, 185–195. [[CrossRef](#)]
51. Molnar, P.; Burchfiel, B.C.; Liang, K.Y.; Zhao, Z.Y. Geomorphic evidence for active faulting in the Altyn Tagh and northern Tibet and qualitative estimates of its contribution to the convergence of India and Eurasia. *Geology* **1987**, *15*, 249–253. [[CrossRef](#)]
52. Zhang, J.X.; Yu, S.Y.; Li, Y.S.; Yu, X.X.; Lin, Y.H.; Mao, X.H. Subduction, accretion and closure of Proto-Tethyan Ocean: Early Paleozoic accretion/collision orogeny in the Altun-Qilian-North Qaidam orogenic system. *Acta Petrol. Sin.* **2015**, *31*, 3531–3554.
53. Xu, B.; Hou, Z.Q.; Zheng, Y.C.; Wang, R.; He, M.Y.; Zhou, L.M.; Yang, Y. In situ elemental and isotopic study of diorite intrusions: Implication for Jurassic arc magmatism and porphyry Cu-Au mineralization in southern Tibet. *Ore Geol. Rev.* **2017**, *90*, 1063–1077. [[CrossRef](#)]
54. Zhang, Y.Q.; He, D.F.; Wu, B.; Gao, H.H. Kinematic evolution of fold-and-thrust belts in the Yubei-Tangbei area: Implications for tectonic events in the southern Tarim Basin. *Geosci. Front.* **2021**, *12*, 101233. [[CrossRef](#)]
55. Kuang, X.T.; Zhu, X.Y.; Ning, F.X.; Li, W.; Zheng, Q.F.; Li, B.; Zhou, D.Q. Aeromagnetic-imaged basement fault structure of the eastern Tarim Basin and its tectonic implication. *Front. Earth Sci.* **2022**, *9*, 825498. [[CrossRef](#)]
56. Shi, G.H.; Jia, R.; Santosh, M.; Liang, H.; He, H.Y. First report of nephrite jade deposit from Africa: Characterization and geological and archeological implications. *GSA Bulletin*. *submitted*.